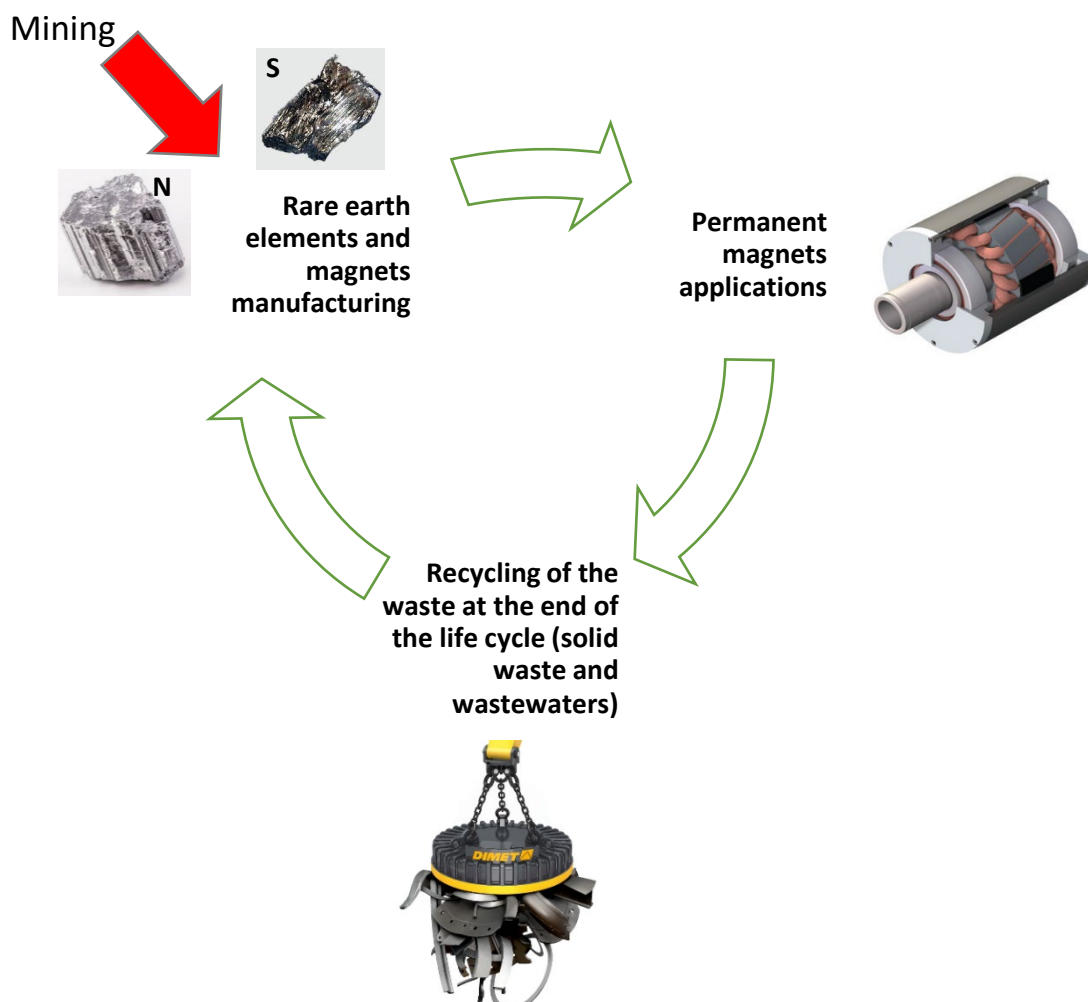




ÅForsk report Grant No. 21-75

Separation and recycling of rare earth elements, cobalt and nickel from magnets



Gulaim Seisenbaeva, Swedish University of Agricultural Sciences

Uppsala, 22 August 2023

Keywords: Critical elements, Recycling, Sustainable Technology, Nanoadsorbents, Functional Ligands, Molecular Models

Summary

Recycling of rare earth elements (REE) is on the way to become an urgent problem in the view of upcoming transfer to electric cars as major means of transportation. The target materials for recycling are electrodes for nickel metal hydride batteries and nickel-neodymium and cobalt-samarium magnets. In the present project we develop high-capacity nanostructured solid adsorbent materials with capacity to efficiently separate REE and 3d Late Transition Metals (LTM) in one step. Their surface layers have been functionalized with highly specific ligands offering possibility of molecular recognition of different metal cations and their separation with high selectivity. The active adsorption sites have been selected from S- and N-donor functional groups, so called "soft bases" to selectively target LTM in the presence of REE. Complexation mechanisms were followed by X-ray spectroscopy and advanced microscopy techniques and visualized using structural studies of relevant molecular models. Functional layers were produced and investigated. Silica nanoparticles for potential use in chromatographic separation were produced and evaluated. Bio-based polymer matrices, such as nano cellulose, have also been studied as sustainable potentially biodegradable alternative to silica.

Contents

1. Introduction	5
2. Synthesis and characterization of matrix materials	5
2a. Silica matrices	5
2b. Nano cellulose matrices	6
3. Surface functionalization of nanoadsorbents	6
3a. Ligand grafting on silica matrices	6
3b. Functionalization of cellulose materials	8
4. Functional characterization of obtained nanomaterials	9
5. Mechanistic insights from the study of molecular model compounds	13
6. Conclusions	15
7. References (including publication of the project results)	15

1. Introduction

The project aims to resolve a principal and highly important problem in recycling of Rare Earth Elements (REE) from the materials that are subject of most urgent request for future industrial development in the world. The problem needs to be principally solved within the next 4-6 year period to secure the future progress of automotive and energy production industries. Solid phase extraction exploiting formation of new types of specific surface complexes, targeting distinct metal cations offers a principally new, and potentially competitive and environmentally friendly solution to this challenge. Many groups in Europe [1, 2] and US [3] joined the race in developing this track. The applicant has developed in the last decade several competitive solutions for metal uptake and separation. Separation of late 3d elements and REE is recognized as a principal bottleneck, requiring new thinking in creation of adsorbent materials. Reaching this goal can provide key advantages for Swedish industries, in particular, Nilar AB and Northvolt AB, that produce REE based materials and are strongly interested in new principally more environmentally friendly recycling technologies.

2. Synthesis and characterization of matrix materials

Matrices for nano adsorbent materials must be cost-efficient to prepare, easy to functionalize and environmentally benign, not to pose environmental or health risks in case of their leakage. In our original project plan we focused on optimization of silica based materials. Increased interest in the society to so-called “green” materials turned our attention also to bio-based and biodegradable nano cellulose matrices.

2a. Silica matrices

In this work, the preparation of dense silica particles has been optimized, applying Sol-Gel approach generally called as Stoeber method [4]. Highly uniform spherical particles an average particle size of 100 nm were produced in water-alcohol solutions by hydrolysis of tetra-ethoxy-silane using aqueous ammonia as basic catalyst (see Fig.1).

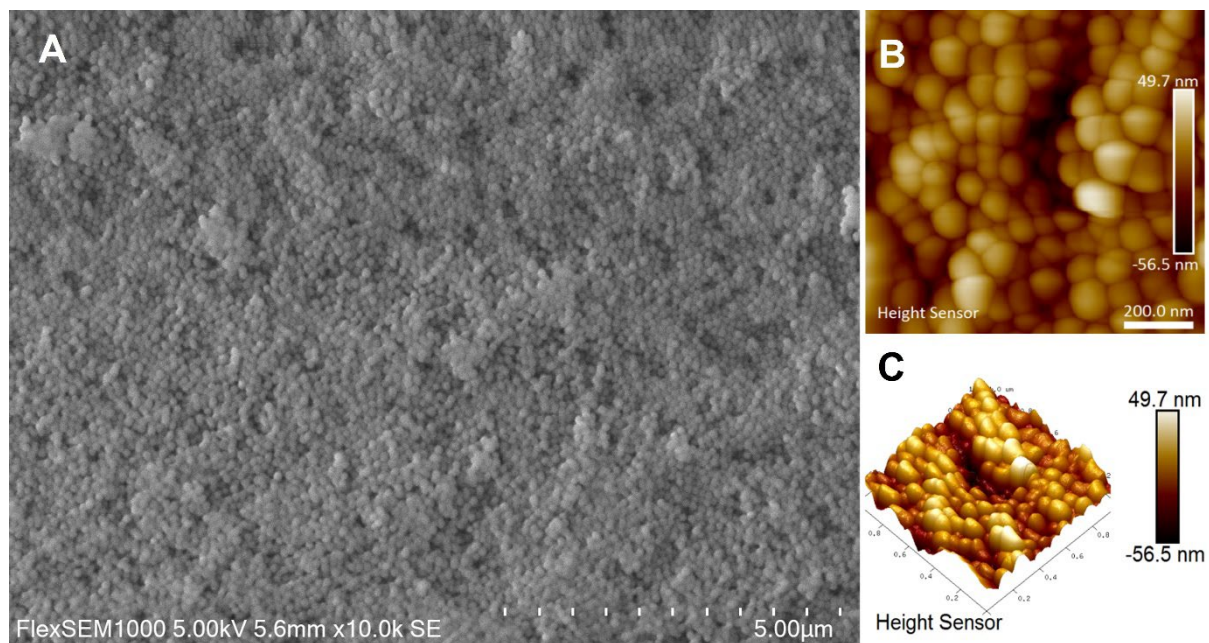


Figure 1. SEM (A) and AFM (B & C) images of typical dense silica particles produced in this project.

The synthesis of mesoporous silicas was following a block-copolymer template approach, optimized for producing so-called SBA type materials and using cost-efficient precursor sodium metasilicate [5] (See Fig. 2).

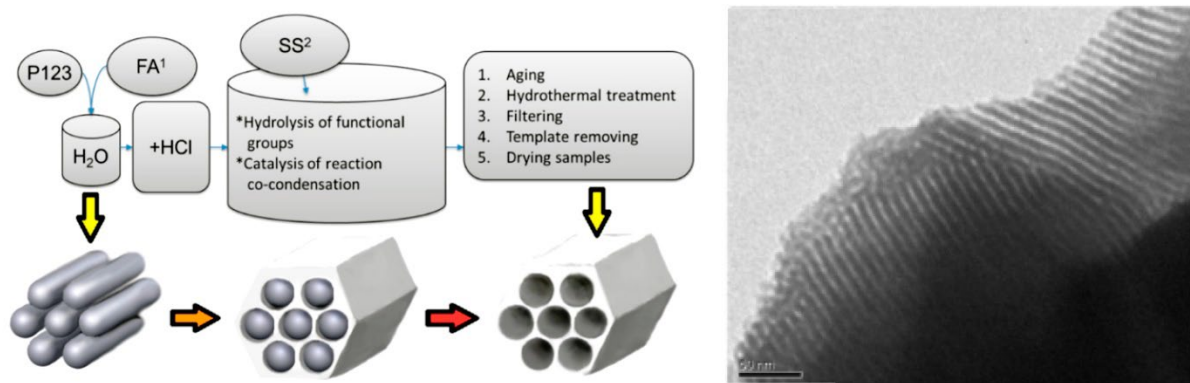


Figure 2. Strategy summary for block-copolymer based approach to SBA-materials and a TEM view of the produced mesoporous structure.

2b. Nano cellulose matrices

Cellulose is the most abundant bio-based polymer on earth, being major component of the plant cell walls and many kinds of bacterial biofilms. Nano cellulose can be obtained in the form Cellulose Nano Fibers (CNF), commonly obtained from wood sources, Cellulose Nano Crystals (CNC) that can be produced from cotton and other fibrous plant materials, and long wires or mats that are obtained from bacterial biofilms. We have selected CNC as target materials in the view of their easy dispersion and high surface area. The synthetic methodology was adapted from [6], optimizing the synthetic conditions (See Fig. 3).

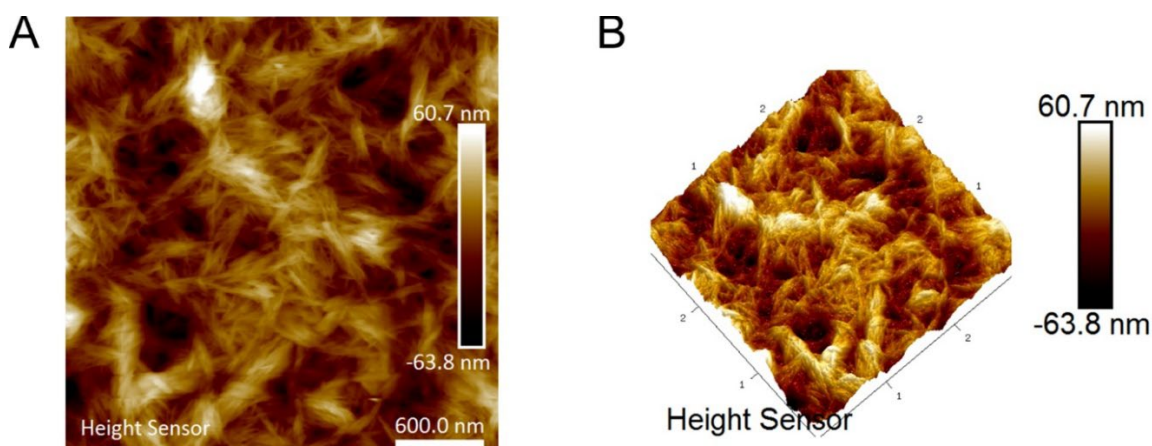


Figure 3. AFM image of a typical sample of CNC nanocrystals produced in this work (A – 2D view, B – 3D view).

3. Surface functionalization of nanoadsorbents

Functionalization approaches can generally be subdivided into 2 groups, where the first one is using a single functional precursor species, while the second is applying step-by-step functionalization. Both these approaches have been investigated and optimized for silica matrices, while only the second one appeared suitable for nano cellulose materials not to involve additional silica components.

3a. Ligand grafting on silica matrices

Grafting of functional alkoxy silanes was carried out in a one step reaction since all the ligands contained organosilane groups (trimethoxysilane or triethoxysilane). The selected precursors (see Fig. 4) have not been used earlier in production of adsorbent materials, but, due to their application in the synthesis of siloxane polymers, were commercially available. Solvent compositions for ligand grafting have been optimized, comparing the products obtained in parent alcohol, toluene or alcohol-toluene mixtures. To enhance the surface reactivity of

particles they have been activated by additional step of washing the synthesized nanoparticles with 1 M nitric acid for 1 hour before the functionalization step. Materials, involving these ligands and produced in the project were reported in [7]. The efficiency of ligand grafting was proved by vibration spectroscopy, TGA studies and X-ray Energy Dispersion Spectroscopy (EDS) analysis (including both gross values and 2D element mapping using Hitachi FlexSEM-1000-II scanning electron & X-ray microscope).

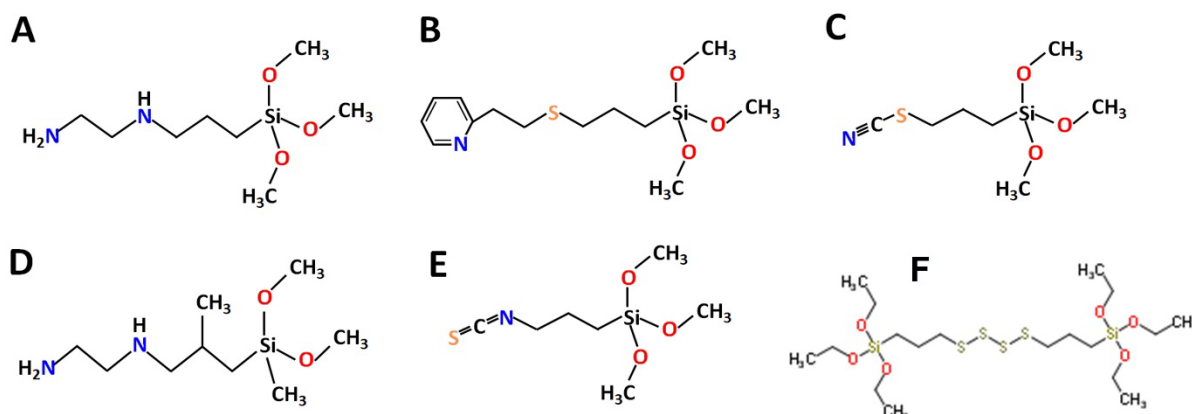


Figure 4. Chemical structure of selected ligands: A-L1, B-L2, C-L3, D-L4, E-L5, F-L6.

The ligands were featuring N- and S-donor functions, potentially selective towards LTM, but not REE.

For **L3** and **L5** ligands the TGA analysis showed double increase in the amount of the grafted ligands after acid wash, while for **L4** the grafted ligand amount remained unchanged. **L4** as well as **L1** are nucleophiles and since amines are basic, a self-catalyzed condensation reaction would be expected, hindering dense attachment on the SiO₂ NPs surface. However, in case of **L4**, possibly faster reacting ligand undergoes homo-condensation instead of condensing with SiO₂ NPs, resulting in formation of clusters, which would be washed out during the washing step.

Table 1. Amount of grafted ligands on SiO₂ NPs.

Sample	Amount of grafted ligand (%)	Amount of grafted ligand (mmol/g)
SiO ₂ _L1	23,45	1,61
SiO ₂ _L2	10,32	0,45
SiO ₂ _L3	9,28	0,63
SiO ₂ _L4	9,24	0,54
SiO ₂ _L5	9,62	0,65
SiO ₂ _L3_acid	15,42	1,02
SiO ₂ _L4_acid	9,23	0,54
SiO ₂ _L5_acid	15,86	1,07

The alternative strategy has been investigated via grafting of iodopropyl trimethoxysilane in the first step with subsequent reactions involving poly-amines, such as diethylene-triamine (DETA) in dimethylformamide as solvent with or without addition of basic catalysts. About 70% substitution of the iodide function with polyamino one was possible to achieve.

In order to enhance selectivity of polyamino ligands resembling L1 and L4, an aromatic ring has been introduced in the ligand structure, see Fig. 5.

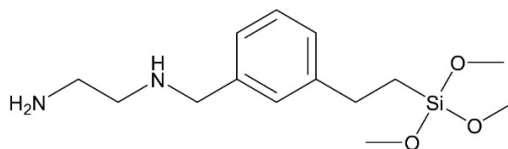


Figure 5. Chemical structure of the diamino ligand bearing an aromatic function [8].

3b. Functionalization of cellulose materials

Cellulose polymer contains as the surface functions only hydroxyl groups, possessing rather limited capacity to interact directly with metal cations. To create surface functions selective for the LTM cations, the produced nano cellulose particles were first chlorinated and then aminated using polyamino functions, such as, for example, tris(aminoethyl)amine, TAEA (see Fig. 6). Produced materials obtained in this project were reported in [9]. The chlorination achieved the yield of ca. 0.8 mmol/g and subsequent amination was in this case essentially quantitative.

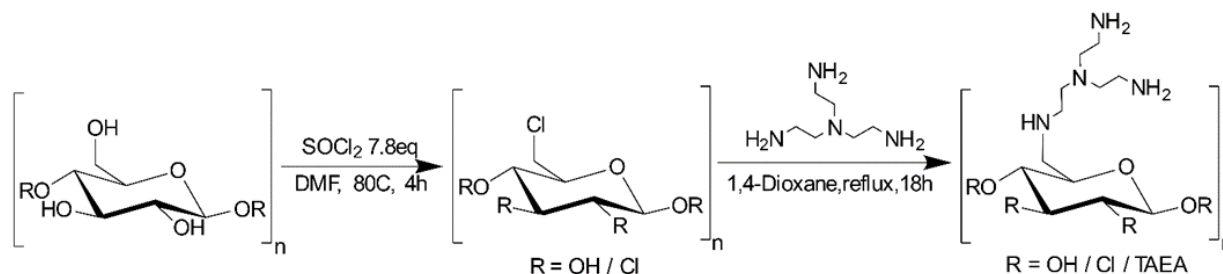


Figure 6. Synthetic route for producing tris(2-aminoethyl)amine modified cellulose.

Interestingly, the surface modification led to considerable changes in the morphology of produced cellulosic materials (see Fig. 7).

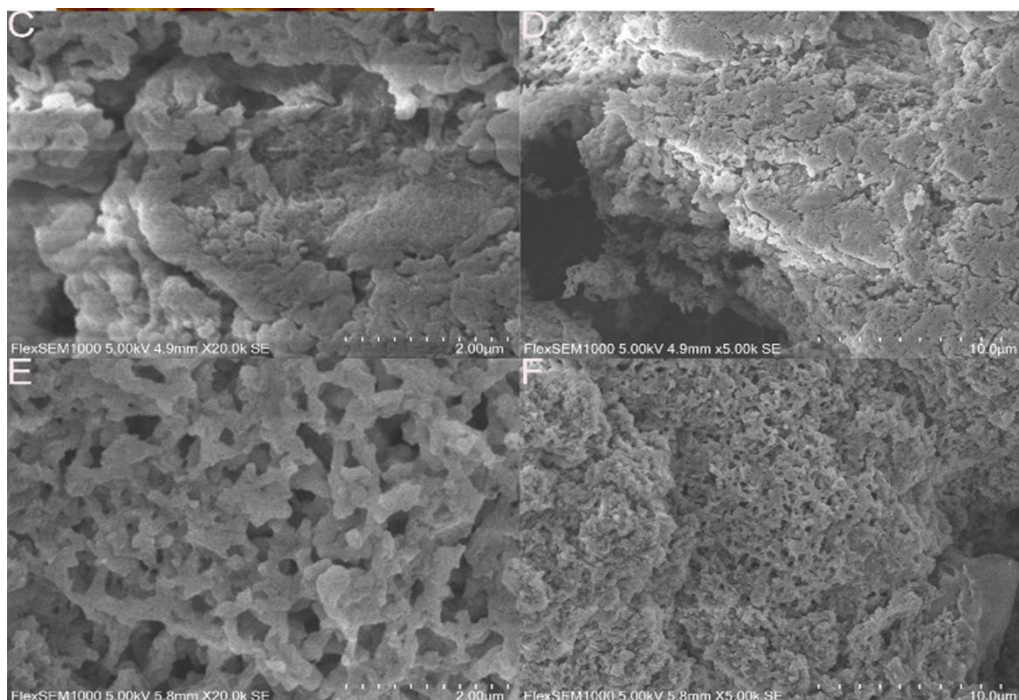


Figure 7. Scanning Electron Microscopy images of Chlorinated CNC derived from cotton CNCs in DMF (C,D) and TAEA-aminated cellulose (E,F).

4. Functional characterization of obtained nanomaterials

In characterization of the obtained materials the focus was set on characterization of both thermodynamics and kinetics of adsorption for individual metal cations and testing selectivity in combinations of metal cations in solutions, typically Nd together with Ni and Sm together with Co, reflecting the principal challenges in separation in the recycling processes. The completeness of desorption and potential selectivity on desorption were also investigated by analysis of both adsorbents (EDS spectroscopy) and solutions (complexometric titrations and EDS on dried samples).

The adsorption thermodynamics was studied via investigation and matching of the adsorption isotherms with most broadly proposed Langmuir and Freundlich models. The Langmuir adsorption isotherm suggests that uptake occurs on a homogeneous surface by monolayer sorption without interactions between adsorbed molecules. The non-linear and linear forms of Langmuir equation can be written as:

$$\frac{C_e}{q_e} = \frac{1}{q_{max}K_L} + \frac{C_e}{q_{max}} \text{ (linear equation)} \quad q_e = \frac{K_L q_{max} C_e}{1 + K_L C_e} \text{ (nonlinear equation)}$$

where C_e is the equilibrium concentration of metal ions (mg/L), q_e is the amount of metal adsorbed per specific amount of adsorbent (mg/g), q_{max} is the maximum adsorption capacity of adsorbent (mg/g) and K_L is an equilibrium constant that reflects the affinity between the adsorbent and adsorbate (L/mg). The values of q_{max} and K_L were calculated by, both, linear (from the slope and intercept of the linear plot of C_e/q_e versus C_e) and non-linear (by Originpro 9) methods.

The Freundlich adsorption isotherm describes reversible and multilayer adsorption on a heterogeneous surface, where the adsorbed amount increases with the concentration according to the following non-linear and linearized equations:

$$\ln q_e = \ln K_f + \frac{1}{n} \ln C_e \text{ (linear equation)} \quad q_e = K_f C_e^{1/n} \text{ (nonlinear equation)}$$

where q_e is the amount of metal ions adsorbed per unit mass of sorbent (mg/g), K_f is the Freundlich constant related to the adsorption capacity (mg/g), C_e is the concentration of adsorbate in the solution at equilibrium (mg/L) and n is related to the adsorption intensity of the adsorbent (L/mg). In the linear form of Freundlich isotherm, the slope and the intercept of the plot of $\ln q_e$ versus $\ln C_e$, correspond to $1/n$ and K_f , respectively. Same values were also calculated via non-linear fitting analysis.

The effect of the concentrations of LTM (Co and Ni) and of RE³⁺ (Nd and Sm) on the adsorption efficiency was investigated in batch studies at room temperature. The results showed that the adsorbed amount of metal ions on grafted SiO₂ NPs increased with increasing the initial metal concentration and reached to the maximum adsorption capacity at higher concentrations due to saturation of the binding sites (Figure 6). The maximum adsorption capacities are summarized in Table 2. Based on the results, SiO₂_L1 demonstrated higher adsorption capacities for all LTM and REEs, which is in agreement with TGA results, considering the grafted amount of the ligands per unit mass of SiO₂ NPs was higher compared to SiO₂_L2 and SiO₂_L3. Both SiO₂ with **L2** and with **L3** had similar maximum adsorption capacities for most of the metal ions, only for Co adsorption SiO₂ NPs grafted with **L3** ligands demonstrated slightly higher adsorption capacity. However, acid treated SiO₂ with **L3** (SiO₂_L3_acid) and **L5** (SiO₂_L5_acid) showed improved adsorption by increasing their maximum capacities twice for Co, Nd, Sm and almost 5 times in case of Ni. According to the literature on coordination chemistry, sulfur and amine containing groups possess higher selectivity towards LTM which can explain higher adsorption capacities towards Ni and Co for most of these ligands.

Table 2. Maximum adsorption capacities of grafted SiO₂ NPs towards REEs and LTM.

	Ni (mmol/g)	Co (mmol/g)	Nd (mmol/g)	Sm (mmol/g)
SiO ₂ _L1	1,66	1,83	0,83	1,1
SiO ₂ _L2	0,55	0,66	0,5	0,56

SiO ₂ _L3	0,58	0,75	0,67	0,66
SiO ₂ _L4	0,57	0,67	0,44	0,77
SiO ₂ _L5	0,34	0,68	0,44	0,68
SiO ₂ _L3_acid	1,00	1,33	0,75	0,83
SiO ₂ _L5_acid	1,66	1,33	0,75	1,00

To understand the adsorption mechanism pathways and characterize the adsorption equilibria, the experimental data were interpreted by linear and non-linear Langmuir (Figure 8) and Freundlich sorption isotherms and the corresponding parameters were summarized in Table 3. Consistent with the correlation coefficient (R^2) values, Langmuir model showed better fit both in linear and non-linear forms, suggesting that the adsorption was a monolayer process on the surface of functionalized silica nanoparticles.

Table 3. List of parameters obtained from Langmuir and Freundlich linear isotherm models

Model		L1	L2	L3									
		Co ⁺²			Ni ⁺²			Sm ⁺³			Nd ³⁺		
Langmuir	q _m	1.90	0,86	0,83	1.82	0.62	0.60	1.31	0.64	0.78	1.12	0.6	0.86
	K _L	0.35	0.14	0.38	0.48	0.37	0.88	0.27	0.36	0.27	0.16	0.26	0.16
	R ²	0.99	0.98	0.99	0.98	0.99	0.99	0.99	0.99	0.99	0.99	0.99	0.99
Freundlich	K _f	0.43	0.09	0,19	0.47	0.13	0.25	0.23	0.16	0.17	0.14	0.12	0.11
	n	2.06	1.40	1.96	2.15	1.90	3.41	1.71	2.27	1.96	1.56	1.85	1.59
	R ²	0.95	0.96	0.91	0.89	0.87	0.92	0.95	0.98	0.95	0.97	0.97	0.98

Summary of adsorption isotherms for the four studied cations and selected ligand functionalized particles is presented in Fig. 8.

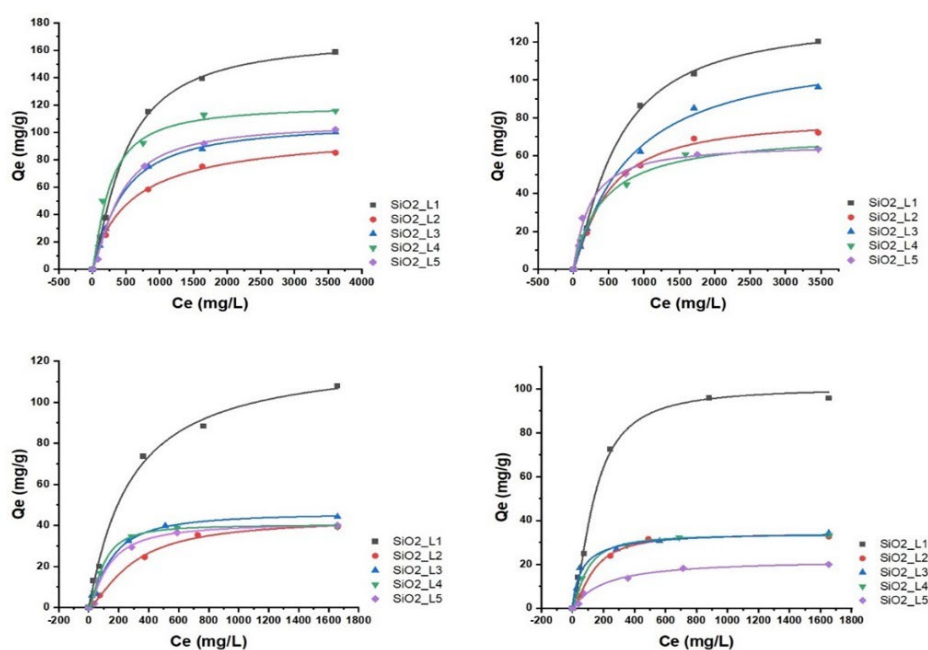


Figure 8. Langmuir adsorption isotherms of A) Sm, B) Nd, C) Co and D) Ni ions onto functionalized silica nanoparticles.

A typical feature of all silica-based adsorbents was rather quick kinetics of uptake of metals with over 60% of the equilibrium capacity being achieved within the first 2 h of adsorption (see Fig. 9).

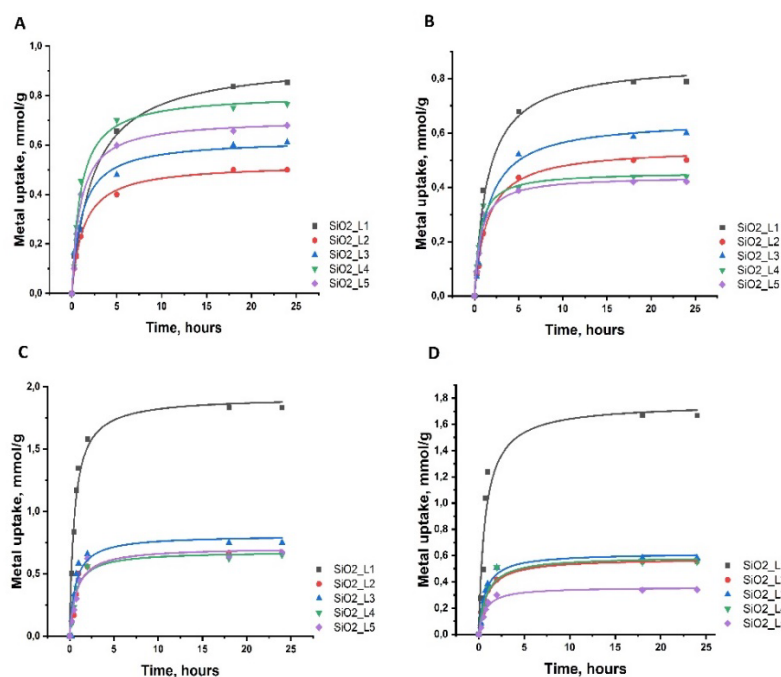


Figure 9. Adsorption kinetics of A) Sm, B) Nd, C) Co and D) Ni onto functionalized silica nanoparticles.

The effect of functionalization conditions turned to be very appreciable for ligand L6. It was best grafted when ethanol was used as solvent in contrast to other ligands, where carrying out the process in toluene turned most fruitful (see Fig. 10).

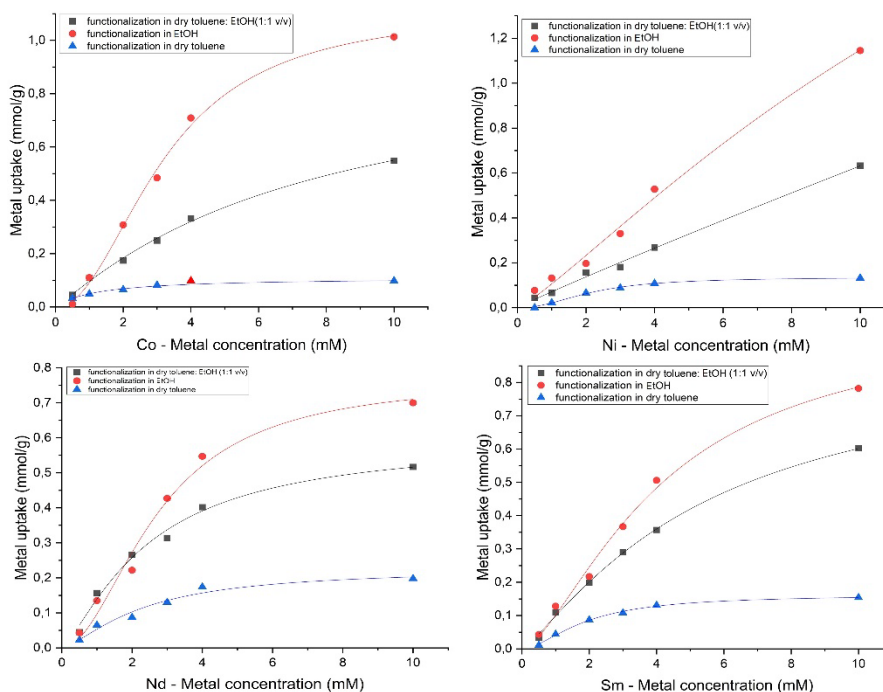


Figure 10. Comparison of the isotherm adsorption curves after functionalization with sulfur containing ligand TESPTS in different solvents (dry toluene - blue line, ethanol - red line, and mixture of dry toluene and ethanol - black line).

The adsorbent produced with a ligand, bearing an aromatic ring revealed strongly enhanced adsorption capacity towards LTM and appreciable selectivity versus LTM in comparison to REE, see Fig. 11. The adsorption kinetics was quick with achieving over 70% of equilibrium capacity in less than 1 hour.

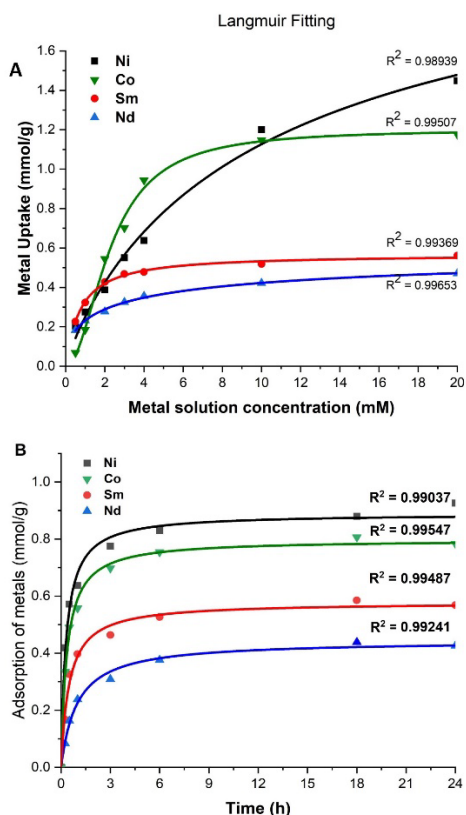


Figure 11. (A): Adsorption isotherms fitted with Langmuir model. (B): adsorption kinetics fitted with the pseudo-2nd order model for prepared nanoadsorbent material.

Adsorption of investigated metal cations on cellulose-derived nanomaterials was generally also following Langmuir isotherms. The average grafted ligand to adsorbed cation ratio was close to 1:1 and the adsorption capacity was achieving approximately 0.8 mmol/g (see Fig. 12).

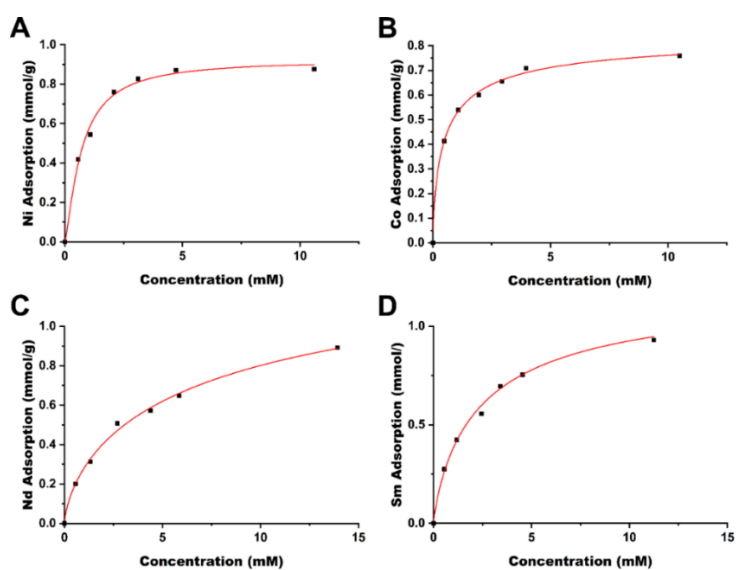


Figure 12. Adsorption isotherms of late transition metals A) Ni, B) Co and rare earth elements C) Nd and D) Sm on TAEA grafted nano cellulose (Best approximated by Langmuir equation).

5. Mechanistic insights from the study of molecular model compounds

For investigation of the potential mechanisms of adsorption we investigated complexation between the target cations and the molecules representing the applied function. New interesting observations have been obtained for TAEA ligand (reported in [9]). In order to produce target complexes, the solutions of corresponding metals as nitrate salts were prepared in milliQ water, followed by the addition 1 molar equivalent of ligand and the solutions allowed to slowly evaporate at room temperature in ca. 50% humidity, producing in case of Ni(II) violet block-shaped crystals. The crystallization residue had very uniform appearance, indicating complete conversion into a single complex form. In case of Co the product after pH-adjustment was a crop of bright red uniform crystals.

The single crystal X-ray study revealed for Ni(II) a molecular structure (see Fig. 13), where the the cation is octahedrally coordinated with the coordination sphere composed of the four nitrogen atoms of the TAEA ligand, one oxygen atom of the coordinated water molecule and one more oxygen atom from the inner-sphere coordinated nitrate ion. The bond lengths are essentially equivalent for all the Ni-N contacts (Ni(1)-N(2) 2.085(6), Ni(1)-N(3) 2.109(6), Ni(1)-N(4) 2.072(6), Ni(1)-N(5) 2.095(6) Å) and the coordinated nitrate oxygen atom (Ni(1)-O(1) 2.101(5) Å). The bond to hydrating water molecule is considerably longer, Ni(1)-O(1B) 2.201(5)Å, which is a commonly observed feature. Bonding within the Ni(TAEA)-fragment is comparable with that observed earlier in the structures of Ni(II) with this ligand such as Ni(TAEA)(NO₃)₂ [10] and [Ni₃(TAEA)₄(H₂O)₂(TMEDA)₂]Cl₆ [11]. In these latter structures the nature of bonding was very analogous with essentially equal bonds to the five neighbours, four N-atoms of the TAEA ligands in both cases (Ni-N 2.055-2.095 and 2.080-2.117 Å respectively) and to one more atom – either O-atom in one of the nitrate ligands or N-atom of the additional TMEDA ligand (2.075 Å in both cases). The sixth bond is much longer and stays for bonding either to an oxygen atom in additional nitrate ion, or to that in a water molecule. Observation of this manner of bonding actually is rather peculiar, indicating most probably Jahn-Teller effect in the 3d⁸ configuration of Ni(II) cation, resulting in weakening of one bond in the octahedral coordination sphere permitting facile ligand exchange between hydrating water and nitrate ligand.

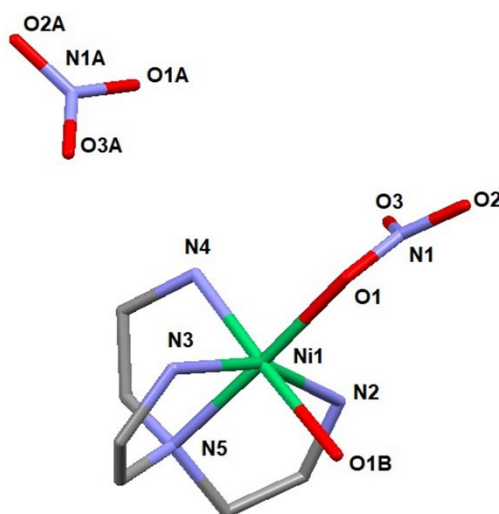


Figure 13. Molecular structure of [Ni(TAEA)(H₂O)(NO₃)](NO₃) (1) [9].

Crystallization in more humid environment in this case led to a structure with the water molecule included in the coordination sphere and “free” nitrate ion. The late transition metal cations (an analogous Co(II) structure has been reported with two nitrite ligands bound in the coordination sphere via N-atoms, Co(TAEA)(NO₂)₂ – all bonds essentially equal in length) are apparently forming stable complexes with the chelating TAEA ligand, which explains stronger selectivity of bonding towards Ni(II) and Co(II) compared to REE of the reported adsorbent.

The crystalline product of Co(II) nitrate interaction with the adsorbent turned out to be a derivative of Co(III) in 3d⁶ configuration, known for crystal field rendered kinetics, which explains the slower desorption of cobalt from the adsorbent on recovery, compared to nickel. The coordination of the Co³⁺ cation is octahedral with 4 positions occupied by the nitrogen atoms of the ligand, where N(1) provides for the tertiary amino function and N(2), N(3)

and N(4) – for the primary amino functions. The residual two places in the inner coordination sphere are occupied by a solvating water molecule O(1) and an oxygen atom of directly bound nitrate anion O(11). An important feature is that all the bonding distances are much shorter compared to Ni²⁺ and are very close to each other except for a considerably longer bond to the solvating water molecule: Co(1)-N(1) 1.919(6), Co(1)-O(11) 1.924(5), Co(1)-N(3) 1.930(12), Co(1)-N(2) 1.938(10), Co(1)-N(4) 1.966(9), and Co(1)-O(1) 1.970(10) Å. This indicates formation of the low-spin 3d⁶ electron configuration, characterized by strong metal-ligand bonding and high activation energy of ligand exchange – a potential hinder for Co³⁺ cation desorption at low pH (see Fig. 14).

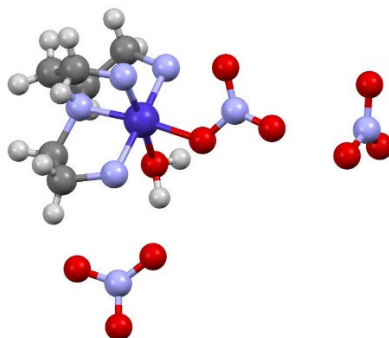


Figure 14. Molecular structure of the complex [Co(H₂NC₂H₄)₃N(H₂O)(NO₃)](NO₃)₂ (**2**) [8].

In case of REE, the product of mass crystallization from equimolar mixture of metal nitrate and TAEA ligand turned out to be solely [N(C₂H₄NH₃)₃](NO₃)₃ (**2**) (see Fig. 15). The nature of the obtained product was the same for both Dy(III) and Sm(III) as indicated by unit cell parameters determinations for multiple single crystals from the reaction mixture. In competition between ligands the Ni(II) cations were binding exclusively to nitrogen atoms in TAEA and REE – to the carboxylate oxygen atoms. Such behavior is well in line with Pearson hard and soft acid-base theory [12] as Ni(II) is a soft acid binding to soft amino ligand, while REE cations are typical hard acids binding to hard oxygen donor bases.

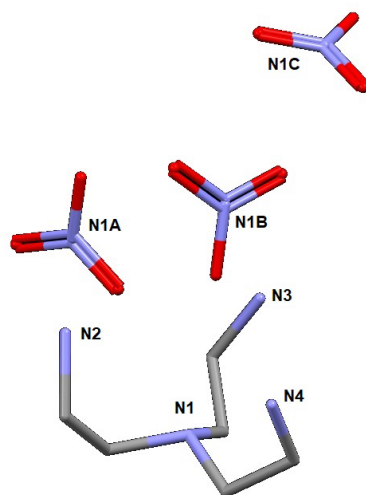


Figure 15. Molecular structure of [N(C₂H₄NH₃)₃](NO₃)₃ (**3**).

The structure of the complex with ligand bearing an aromatic function featured symmetric attachment of two ethylene diamine donor functions to the Ni(II) cation connected to outer-sphere nitrate anions via hydrogen bonds to solvating water molecules. Coordination of the nickel cation is octahedral with four nitrogen atoms in the equatorial plane and two hydrating water molecules in the axial positions. The square planar arrangement in this case is apparently not associated with low-spin coordination of Ni(II) or any Jahn-Teller distortion, as the

bond length to the nitrogen atoms 2.076(2) and 2.130(2) Å are apparently comparable with the bond length to the solvating water molecules, 2.107(2) Å, see Fig. 16.

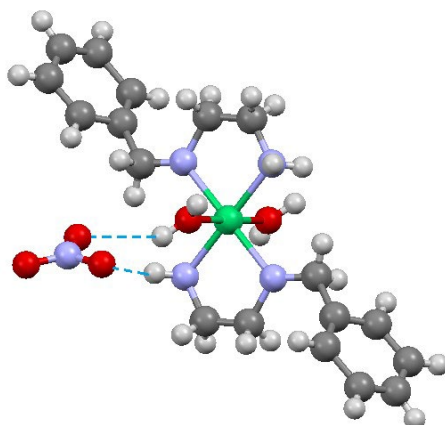


Figure 16. Molecular structure of the complex $[\text{Ni}(\eta^2\text{-H}_2\text{NC}_2\text{H}_4\text{NHCH}_2\text{C}_6\text{H}_5)_2(\text{H}_2\text{O})_2](\text{NO}_3)_2$ (**4**). Only one hydrogen bonded nitrate anion is displayed for clarity.

No X-ray quality crystals could be obtained for the Co-derivative, but the data of UV-Vis and XPS spectroscopy clearly indicated even in this case oxidation of Co(II) into Co(III), explaining again better retention of cobalt compared to nickel on the produced adsorbent.

6. Conclusions

The research results produced in the project are highly promising and confirm the working hypothesis aimed at exploiting differences in the coordination chemistry of REE and LTM. Effective adsorbents have been produced and characterized using even a broader selection of carrier matrices. The research aims set in the project have been achieved. It has been demonstrated that using self-assembling ligands bearing aromatic fragment increases the adsorption capacity and offers quick adsorption kinetics. Investigation of molecular mechanisms in adsorption showed principal difference in behavior between REE and LTM and permitted to trace possibility for even separation of LTM from each other.

7. References (including publication of the project results – indicated by *)

- 1) Dupont D., Brullot W., Bloemen M., Verbiest T., Binnemans K., *ACS Appl. Mater. Interfaces*, **2014**, 6, 4980-4988.
- 2) Dupont D., Luyten J., Bloemen M., Verbiest T., Binnemans K., *Ind. Eng. Chem. Res.*, **2014**, 53, 15222-15229.
- 3) Callura J. C., Perkins K. M., Noack C. W., Washburn N. R., Dzombak D. A., Karamalidis A. K., *Green Chem.*, **2018**, 20, 1515-1526.
- 4) Tadanaga K., Morita K., Mori K., Tatsumisago M., *J. Sol-Gel Sci. Tech.*, **2013**, 68, 341-345.
- 5) Dudarko O., Kobylinska N., Mishra B., Kessler V.G., Tripathi B.P., Seisenbaeva G.A., *Micropor. Mesopor. Mater.*, **2021**, 315, 110919.
- 6) Reid M. S., Villalobos M., Cranston E. D., *Langmuir*, **2017**, 33, 1583-1598.
- * 7) Vardanyan A., Guillon A., Budnyak T., Seisenbaeva G.A., *Nanomater.*, **2022**, 12, 974.
- * 8) Lakic M., Breijaert T.C., Daniel G., Svensson F.G., Kessler V.G., Seisenbaeva G.A., *Sep. Purif. Technol.*, **2023**, 323, 124487.
- * 9) Breijaert T.C., Budnyak T.M., Kessler V.G., Seisenbaeva G.A., *Dalton Trans.* **2022**, 51, 17978–17986.

- 10) Matelková K., Moncol J., Herchel R., Dlháň Ľ., Ivaniková R., Svoboda I., Padělková Z., Mašlejová A., *Polyhedron*, **2013**, 56, 1-8.
- 11) Bazzicalupi C., Bencini A., Bianchi A., Danesi A., Giorgi C., Valtancoli B., *Inorg. Chem.*, **2009**, 48, 2391-2398.
- 12) Pearson R.G., *J. Am. Chem. Soc.*, **1963**, 85, 3533–3539.